AIAA JOURNAL
Vol. 34, No. 10, October 1996

Technical Notes

TECHNICAL NOTES are short manuscripts describing new developments or important results of a preliminary nature. These Notes cannot exceed 6 manuscript pages and 3 figures; a page of text may be substituted for a figure and vice versa. After informal review by the editors, they may be published within a few months of the date of receipt. Style requirements are the same as for regular contributions (see inside back cover).

Multiple-Actuator Control of Vortex Breakdown on a Pitching Delta Wing

Peter Vorobieff* and Donald Rockwell†
Lehigh University,
Bethlehem, Pennsylvania 18015-3085

I. Introduction

ALTHOUGH the phenomenon of vortex breakdown on delta wings has been known since the early 1960s, only recently have investigations concentrated on control of the breakdown location on maneuvering delta wings. Quantitative interpretations of the flow patterns via particle image velocimetry during pitching motion are given by Magness et al.[1] and Cipolla and Rockwell.[2] Overviews of the control of vortex breakdown on pitching delta wings from numerical and experimental views are provided by Visbal[3] and Rockwell,[4] respectively. The consequences of unsteady blowing-suction at the leading edge and blowing at the trailing edge, applied to a stationary wing, are described respectively in the investigations of Gu et al.[5] and Helin and Watry.[6] Not yet investigated is simultaneous control applied at the leading and trailing edges during pitching motion of the delta wing.

The present study focuses on the combined effect of leading- and trailing-edge controls on vortex breakdown while the wing is undergoing harmonic pitching motion. The major objective is to exert the maximum influence on vortex breakdown with minimum energy input from the applied controls.

II. Experimental Setup and Technique

A. Experimental Setup

The experiments were conducted in a large-scale water channel constructed of transparent Plexiglas®. The test section was 5.49 m long, 0.62 m wide, and 0.58 m high, with the water level maintained at 0.53 m.

The experimental apparatus consisted of a half-delta wing made of Lexan, which is illustrated schematically in Fig. 1. This wing was rigidly connected to a rotating disk mounted on a vertical Plexiglas plate (false wall). The false wall was used to isolate the zone of the half-delta wing from the influence of the actuating mechanisms driven by four compumotors (computer-controlled high-resolution stepping motors). One compumotor varied the angle-of-attack α via a gear-and-chain drive attached to the rotating disk. Another activated the leading-edge flap, deflecting it to an angle β from the neural position. Two other motors controlled the trailing-edge blowing mechanism: one rotated the hollow brass tube with orifices that was mounted at the trailing edge of the wing, thus changing the angle γ between the direction of the orifices and the centerline of the wing; and the other drove the piston attached to the blowing tube, changing the blowing velocity v_j.

Received Oct. 27, 1995; revision received Feb. 12, 1996; accepted for publication Feb. 28, 1996.

*Research Assistant, Department of Mechanical Engineering.
†Paul B. Reinhold Professor, Department of Mechanical Engineering. Member AIAA.

The compumotor systems were connected to an Intel 80386 computer, which stored information about the profiles of α, β, γ, and v_j and transmitted it to the compumotors, with the details of the arrangement similar to those described by Cipolla and Rockwell.[2]

The geometric parameters of the delta wing were as follows: root chord C, 243 mm; sweep angle Λ of the wing without the flap, 75 deg; sweep angle of the wing with the flap, 72 deg; wing thickness, 12.7 mm; diameter of the trailing-edge blowing tube, 6.35 mm; blowing tube orifice diameter, 0.8 mm; and number of orifices, 37, giving the total area of the blowing nozzles A_j equal to 18.3 mm.[2]

B. Experimental and Data Processing Technique

To visualize the location of vortex breakdown, dye was injected into the leading-edge vortex through a nozzle in the false wall. The results of the experiments were recorded on S-VHS tape and then analyzed frame by frame to determine the time history of the distance between the apex of the wing and the onset of vortex breakdown x_b (see Fig. 1, side view). Twenty measurements per cycle were taken (two per second), with the error in determining the exact location of the onset of vortex breakdown no more than 2 mm (0.8% of chord C). After the time history of x_b was recorded, x_b was ensemble averaged, using six instantaneous values of x_b, which were obtained at the same phase of the pitching cycle of the wing. In plotting data, ensemble-averaged x_b vs α rather than x_b vs time was used to emphasize the hysteresis effect.

III. Experiment and Results

A. General Experimental Conditions

The experiments were conducted at a freestream velocity $U_\infty = 0.144$ m/s, corresponding to Reynolds number $Re = 3.46 \times 10^4$ in terms of chord C. In all of the experiments with pitching, the mean angle-of-attack $\bar{\alpha}$ was 40 deg, the pitching amplitude α_0 was 10 deg,

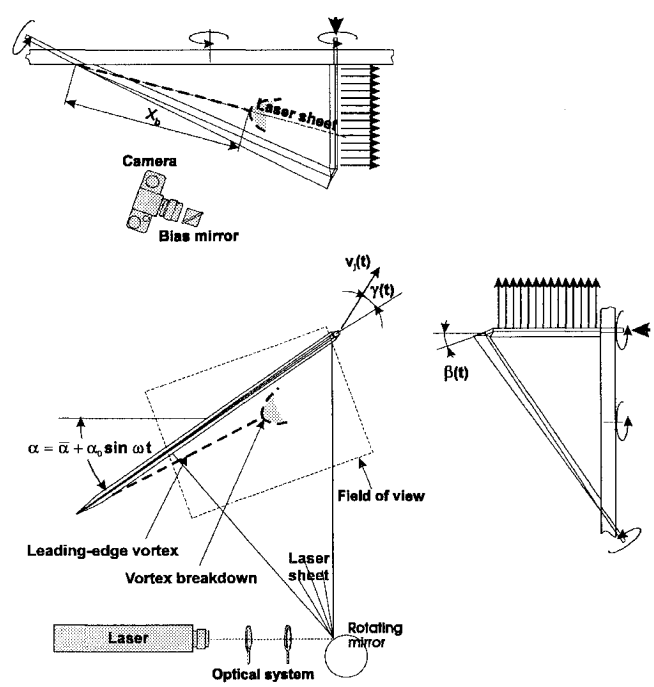

Fig. 1 Experimental apparatus.

and the pitching period $T = 2\pi/\omega$ was 10 s, with sinusoidal pitching $\alpha(t) = \bar{\alpha} + \alpha_0 \sin \omega t$. Pitching and the controls phase-locked to it were activated at least five cycles before video recording started. The resulting dimensionless frequency of oscillation $k^* = \pi C/TU_\infty$ was 0.53.

During the experiments, the leading-edge flap could be deflected by 25 deg upward and downward from its neutral position. Trailing-edge blowing velocity v_j was four times the freestream velocity U_∞.

B. Influence of Leading-Edge Flap Deflection

Preliminary experiments with various phase-locked profiles of flap deflection were conducted; however, maintaining a fixed upward or downward deflection of the flap for the duration of the entire pitching cycle proved to be the most influential. Figure 2 shows that the effect of constant leading-edge flap deflection on vortex breakdown for the case of harmonic pitching (looped curves) is much more prominent than that for the static case, though qualitatively the effect is the same: Upward flap deflection produces retardation of the onset of vortex breakdown; downward flap deflection advances it. For flap oscillation with high frequencies (period less than one-fifth of a pitching period), there is no significant change in the mean breakdown position, whereas flap deflection upward on the upstroke part of the pitching cycle only produces effect close to that of constant upward flap deflection.

C. Influence of Transient Trailing-Edge Blowing

Preliminary experiments investigated different directions and durations of blowing as well as timing of the onset of blowing during the pitching cycle. A blowing angle $\gamma = 30$ deg appeared to be the most effective for the retardation of vortex breakdown; it was employed in all subsequent experiments. To make the blowing more energetically efficient, a limited blowing duration of only 40% of the pitching period, i.e., $0.4T$, was found to be effective.

With the blowing duration fixed at $0.4T$, it was important to optimize the timing of the onset of blowing (Fig. 3). The dimensionless delay $\tau = t_0/T$ defines the time elapsed from the beginning of the sinusoidal pitching cycle to the onset of blowing t_0. Solid lines on the graphs indicate the intervals when blowing was on. Onset of blowing during the downstroke portion of the cycle ($\tau = 0.2$) retards the occurrence of vortex breakdown much less effectively than onset of blowing during the upstroke ($\tau = 0.8$).

Traditional definition of the dimensionless momentum coefficient $c_\mu = (v_j/U_\infty)^2(A_j/S^2)$, where S is the semispan of the wing at the trailing edge, is not adequate to describe the efficiency of blowing in the present case where the blowing velocity v_j is nonzero only during a fraction of the pitching cycle. Instead, we introduce

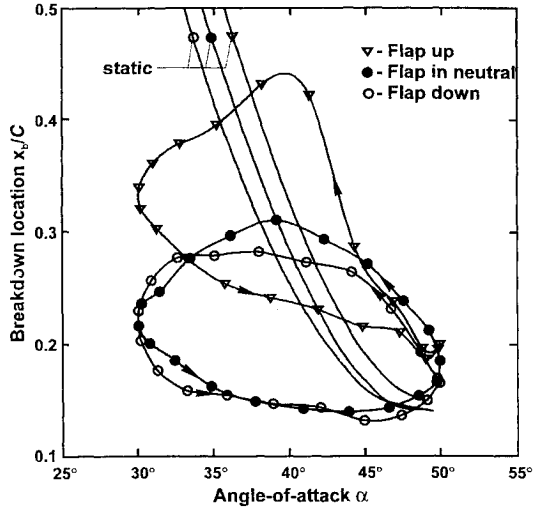

Fig. 2 Influence of leading-edge flap deflection on dimensionless vortex breakdown location x_b/C vs angle-of-attack α.

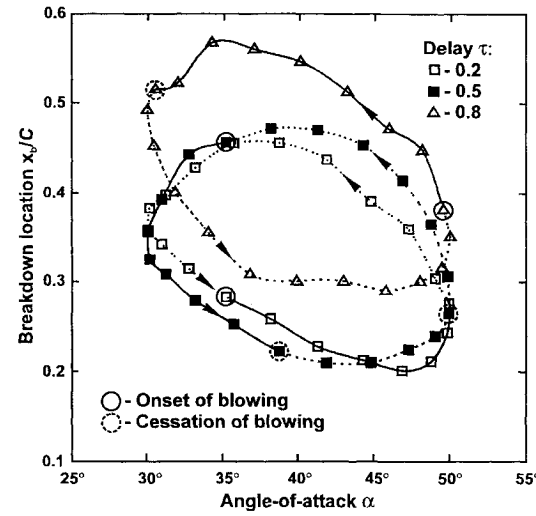

Fig. 3 Influence of trailing-edge blowing on dimensionless vortex breakdown location x_b/C vs angle-of-attack α.

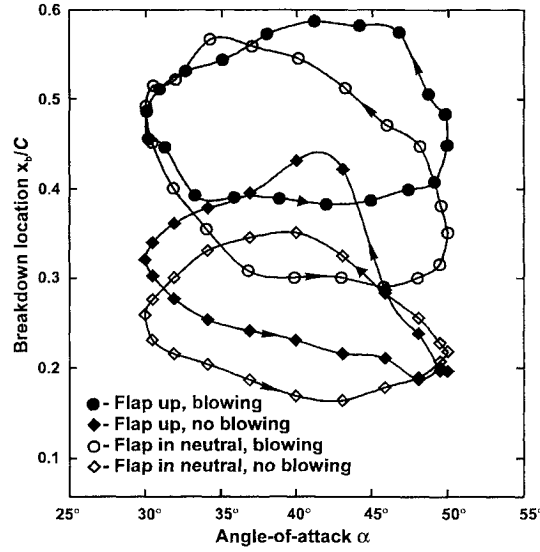

Fig. 4 Control influence summary.

the momentum coefficient time-averaged over one pitching–control application period:

$$\Theta_\mu = \left(\frac{1}{T}\int_0^T |v_j(t)|\frac{dt}{U_\infty}\right)^2 \frac{A_j}{S^2}$$

When the blowing has constant magnitude for all time, $\Theta_\mu = c_\mu$. The value of Θ_μ corresponding to the optimal conditions described in the foregoing was 0.007. Note that this value is substantially less than that typically employed in simulations of the effect of thrust vectoring on vortex breakdown. If, for example, continuous blowing is applied at a velocity $2U_\infty$ through an area corresponding to one-half of the cross section of the trailing edge of the wing, then $c_\mu \approx 1.6$.

D. Cumulative Influence of Trailing-Edge Blowing and Leading-Edge Flap Deflection

Figure 4 illustrates the relative effects of separate and simultaneous application of leading- and trailing-edge controls to the pitching half-delta wing. The effect of trailing-edge blowing during the upstroke with the flap in the neutral position retards the mean onset of breakdown from $0.26C$ to $0.42C$, where C is the chord. The effect of the flap deflection in the absence of blowing is not as strong; it retards the mean onset of breakdown from $0.26C$ to $0.32C$. The most effective is combined trailing-edge blowing and flap deflection, which retards breakdown to $0.49C$.

IV. Conclusions

For the range of the angles of attack studied, the time-averaged mean distance to the onset of vortex breakdown on a pitching delta wing can be extended by nearly 100% with combined deflection of leading-edge flaps and transient trailing-edge blowing, which is invoked during only a fraction of the pitching cycle. Most effective is blowing during the upstroke portion of the cycle. With this approach, the effective momentum coefficient of the blowing is extremely small. Further optimization of controls will require detailed knowledge of the qualitative and quantitative character of the changes in the flow topology caused by the application of leading- and trailing-edge controls. This experiment is currently under way.

Acknowledgments

The authors are grateful to the U.S. Air Force Office of Scientific Research for support of this research under Grant F49620-95-1-0220 monitored by Len Sakell.

References

[1]Magness, C., Robinson, O., and Rockwell, D., "Control of Leading-Edge Vortices on a Delta Wing," AIAA Paper 89-0999, March 1989.

[2]Cipolla, K., and Rockwell, D., "Flow Structure on a Stalled Delta Wing Subjected to Small Amplitude Pitching Oscillations," *AIAA Journal*, Vol. 33, No. 7, 1995, pp. 1256–1262.

[3]Visbal, M. R., "Structure of Vortex Breakdown on a Pitching Delta Wing," AIAA Paper 93-0434, Jan. 1993.

[4]Rockwell, D., "Three-Dimensional Flow Structure on Delta Wings at High Angle-of-Attack: Experimental Concepts and Issues," AIAA Paper 93-0550, Jan. 1993.

[5]Gu, W., Robinson, O., and Rockwell, D., "Control of Vortices on a Delta Wing by Leading-Edge Injection," *AIAA Journal*, Vol. 31, No. 7, 1993, pp. 1177–1185.

[6]Helin, H. E., and Watry, C. W., "Effects of Trailing-Edge Jet Entrainment on Delta Wing Vortices," *AIAA Journal*, Vol. 32, No. 4, 1994, pp. 802–804.

Explicit Algebraic Stress Model of Turbulence with Anisotropic Dissipation

Xiang-Hua Xu* and Charles G. Speziale†
Boston University, Boston, Massachusetts 02215

I. Introduction

TURBULENT flows near solid boundaries—or at low turbulence Reynolds numbers—can exhibit significant anisotropies in the turbulent dissipation rate.[1] Nevertheless, Reynolds stress turbulence closures are routinely formulated that neglect such effects by invoking the Kolmogorov assumption of local isotropy.[2] Recently, however, attempts have been made to extend full Reynolds stress turbulence closures to incorporate the effects of anisotropic dissipation.[3–6] These more sophisticated Reynolds stress turbulence closures can involve the solution of up to 12 additional transport equations. As such, most of these models are not currently feasible for the solution of complex turbulent flows in an engineering setting.

During the past few years, explicit algebraic stress models have been developed that are formally consistent with full second-order closures in the limit of homogeneous turbulence in equilibrium.[7] These models allow for the solution of complex turbulent flows with a substantially reduced level of computation compared with full second-order closures, since they constitute two-equation models.[7,8] The purpose of the present Note is to show how the effects of anisotropic dissipation can be systematically incorporated into these explicit algebraic stress models by a simple readjustment of the coefficients. For homogeneous turbulent flows that are close to equilibrium, it will be shown that the results obtained with such models are virtually indistinguishable from those obtained using a full second-order closure model with the anisotropic dissipation rate model of Speziale and Gatski.[4] All of this extra turbulence physics is incorporated within the framework of a two-equation model that is not much more computationally expensive to implement than the standard K–ε model.

II. Theoretical Background

We will consider incompressible turbulent flows where the velocity v_i and kinematic pressure P are decomposed, respectively, into ensemble mean and fluctuating parts as follows:

$$v_i = \bar{v}_i + u_i, \qquad P = \bar{P} + p \tag{1}$$

In homogeneous turbulence, where all higher-order correlations are spatially uniform, the Reynolds stress tensor $\tau_{ij} \equiv \overline{u_i u_j}$ satisfies the transport equation[9]

$$\dot{\tau}_{ij} = -\tau_{ik}\frac{\partial \bar{v}_j}{\partial x_k} - \tau_{jk}\frac{\partial \bar{v}_i}{\partial x_k} + \Pi_{ij} - \varepsilon_{ij} \tag{2}$$

where

$$\Pi_{ij} \equiv \overline{p\left(\frac{\partial u_i}{\partial x_j} + \frac{\partial u_j}{\partial x_i}\right)}, \qquad \varepsilon_{ij} \equiv 2\nu\overline{\frac{\partial u_i}{\partial x_k}\frac{\partial u_j}{\partial x_k}}$$

are, respectively, the pressure-strain correlation and the dissipation rate tensor. Thus, in homogeneous turbulence, only Π_{ij} and ε_{ij} need to be modeled to achieve closure.

Speziale et al.[10] (SSG) showed that, for two-dimensional mean turbulent flows in equilibrium, the commonly used hierarchy of pressure-strain models simplifies to

$$\begin{aligned}\Pi_{ij} = {} & -C_1\varepsilon b_{ij} + C_2\varepsilon\left(b_{ik}b_{kj} - \tfrac{1}{3}b_{kl}b_{kl}\delta_{ij}\right) + C_3 K\bar{S}_{ij} \\ & + C_4 K\left(b_{ik}\bar{S}_{jk} + b_{jk}\bar{S}_{ik} - \tfrac{2}{3}b_{kl}\bar{S}_{kl}\delta_{ij}\right) \\ & + C_5 K\left(b_{ik}\bar{\omega}_{jk} + b_{jk}\bar{\omega}_{ik}\right)\end{aligned} \tag{3}$$

where

$$\bar{S}_{ij} = \frac{1}{2}\left(\frac{\partial \bar{v}_i}{\partial x_j} + \frac{\partial \bar{v}_j}{\partial x_i}\right), \qquad \bar{\omega}_{ij} = \frac{1}{2}\left(\frac{\partial \bar{v}_i}{\partial x_j} - \frac{\partial \bar{v}_j}{\partial x_i}\right)$$

$$b_{ij} = \frac{\tau_{ij} - \frac{2}{3}K\delta_{ij}}{2K}$$

are, respectively, the mean rate of strain tensor, the mean vorticity tensor, and the Reynolds stress anisotropy tensor; $K \equiv \frac{1}{2}\tau_{ii}$ is the turbulent kinetic energy. The SSG model[10] is a simple extension of Eq. (3) that is valid for moderate departures from equilibrium. It has been found that the nonlinear return term containing C_2 can be neglected without introducing an appreciable error.[7,10] With the choice of constants

$$C_1 = 6.80, \qquad C_2 = 0, \qquad C_3 = 0.36$$

$$C_4 = 1.25, \qquad C_5 = 0.40$$

in Eq. (3), excellent equilibrium values are obtained for the benchmark case of homogeneous shear flow. We refer to this as the linearized, equilibrium form of the SSG model.

The Kolmogorov assumption of local isotropy is typically invoked wherein it is assumed that[2,9]

$$\varepsilon_{ij} = \tfrac{2}{3}\varepsilon\delta_{ij} \tag{4}$$

Received Feb. 3, 1996; revision received June 16, 1996; accepted for publication June 25, 1996; also published in *AIAA Journal on Disc*, Volume 2, Number 1.

*Research Assistant, Department of Aerospace and Mechanical Engineering.

†Professor, Department of Aerospace and Mechanical Engineering. Member AIAA.